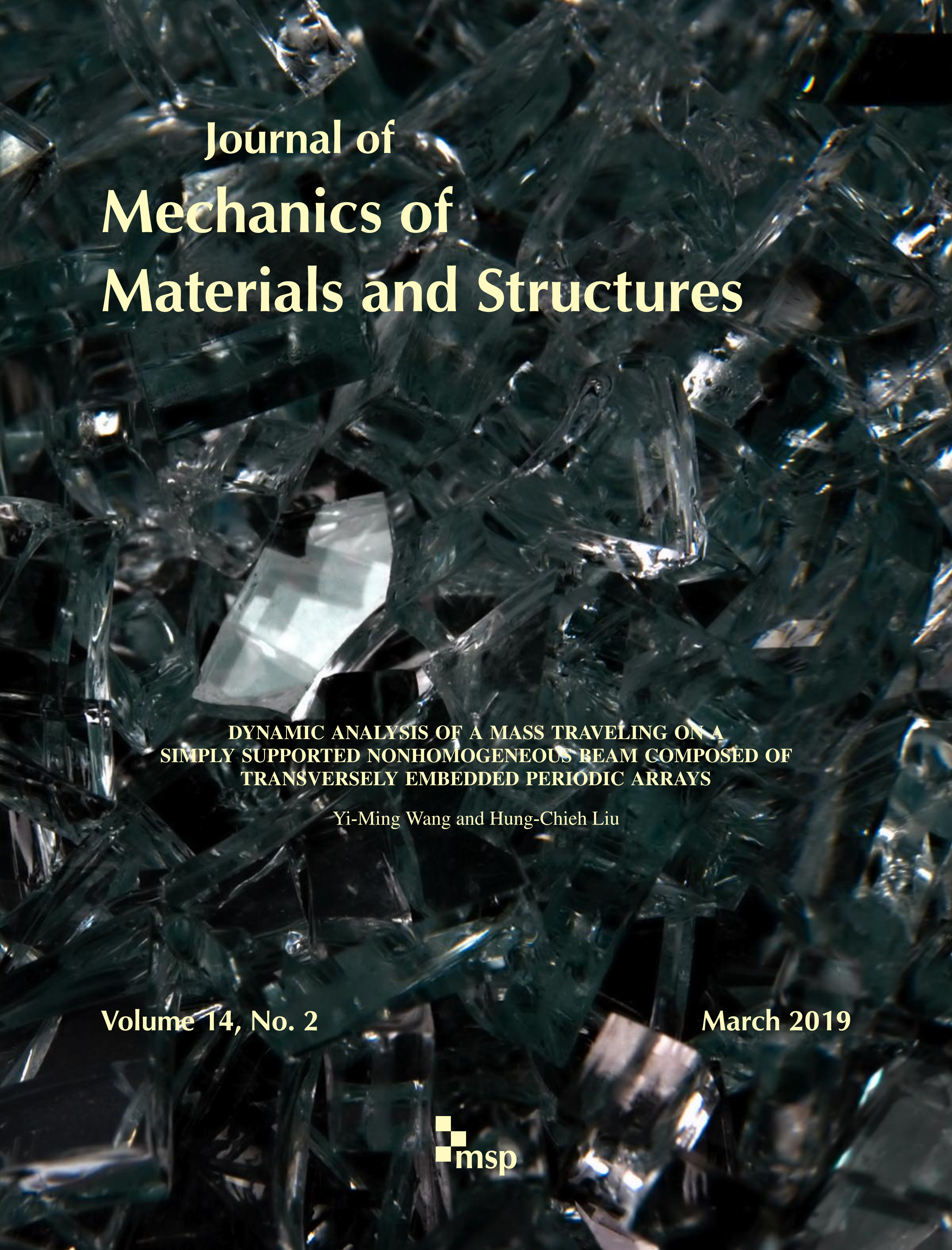

Journal of
Mechanics of Materials and Structures

DYNAMIC ANALYSIS OF A MASS TRAVELING ON A SIMPLY SUPPORTED NONHOMOGENEOUS BEAM COMPOSED OF TRANSVERSELY EMBEDDED PERIODIC ARRAYS

Yi-Ming Wang and Hung-Chieh Liu

Volume 14, No. 2

March 2019

msp

JOURNAL OF MECHANICS OF MATERIALS AND STRUCTURES
Vol. 14, No. 2, 2019
dx.doi.org/10.2140/jomms.2019.14.237

DYNAMIC ANALYSIS OF A MASS TRAVELING ON A SIMPLY SUPPORTED NONHOMOGENEOUS BEAM COMPOSED OF TRANSVERSELY EMBEDDED PERIODIC ARRAYS

YI-MING WANG AND HUNG-CHIEH LIU

Periodically embedded specified materials and laminas into the beam of a beam-mass system to form a stiffness-driven nonhomogeneous beam having the potential to shift its specific stiffness to avoid the happening of large amplitude vibration and resonance is worthy of note. However, if the arrangement of composed materials and layers of the beam is changed, the developed model generally has to be reestablished. To propose a model that can be used to analyze beams consisting of different assemblies of materials and laminas is of great importance. Another point is using specified materials and laminas, which are periodically embedded into a beam to form transversely periodic arrays, to make the beam have the capability to change its specific stiffness to satisfy designing requirement. The Fourier-series based approach is employed to take into account the periodicity of material properties and matching conditions across laminas' interfaces. The influence produced by the arrays to the dynamics of the system is examined.

Result shows that the axial Young's modulus and density of the proposed beam are biaxial periodic functions. Different arrangements of embedded arrays bring different stiffness shifting potential of the beam to reduce the vibration of the system. With proper choice of the stiffness and thickness ratios between the arrays and basic layers, the growth of small amplitude vibration into large motion regime can be attenuated. Meanwhile, by changing the thickness ratios in the width and height directions, there exist seven possible compositions of the beam. It discloses that despite without considering the material damping, the proposed beam still has good ability to diminish the beam vibration even after the mass left the beam.

1. Introduction

Stiffness-driven beam-like members have been widely found in civil and mechanical engineering. Due to high demand of operational safety of structures and mechanical systems, flexible members having the capability to shift their stiffness-to-weight-ratio to avoid the happening of large amplitude vibration are of great importance. For a beam-mass system, if the beam has the potential to vary its transverse frequency, the dynamic response of the system is able to be improved. In other words, short useful life and failure of structures caused by the occurrence of large amplitude vibration can be attenuated.

Mohebpour et al. [2016] studied the dynamics of a mass riding on an inclined symmetric cross-ply laminated beam. Based on classical laminated theory and finite element approach, the equations of motion were derived and solved. Their results indicated that a laminated composite beam had better bending stiffness than a homogeneous beam. Meanwhile, the orientation of the layer had influential effect to the bending stiffness of the composite beam.

Keywords: transversely periodic arrays, stiffness-driven beam, Fourier series, thickness ratio.

Misiurek and Śniady [2013] investigated the dynamics of a force moving at constant speed on a simply supported sandwich beam. A closed-form solution was obtained by the method of superimposed deflections. They pointed out that when the speed of a point force was less and larger than the shear wave velocity of the beam, different forms of the closed-form solutions were presented. Song et al. [2018] made a parametric study to the dynamics of a sandwich plate subjected to a mass moving with constant speed. The composite plate was composed of two isotropic face plates and a viscoelastic inner layer. The effects produced by different boundary constraints were determined. They showed that using nonhomogeneous structural members improved the dynamic behaviors of structures.

Tao et al. [2016] analyzed the dynamics of a fiber metal laminated beam induced by the motion of a riding load and the change of environmental temperature. The beam consisted of three symmetric cross-ply fiber reinforced layers and two metal layers. Their results disclosed that the geometric properties and environmental temperature played key roles to the mid-span response of the beam. Meanwhile, the increase of temperature decreased the bending stiffness of the beam.

Wang [2009] considered the dynamics induced by a mass traveling on a beam having periodic arrays in axial direction. The inhomogeneous beam was assumed to be composed of two different laminas. The Fourier-series based approach was introduced to take over the axial periodicity of the beam. This is also one of the bases of this study.

Sayyad and Ghugal [2017] made an excellent review of existing studies on bending, buckling and free vibration of laminated composite and sandwich beams. They discussed many popular methods that have been applied on the analysis, e.g., finite element approaches based on classical and refined theories, displacement fields of various equivalent single layer, layerwise, and zig-zag theories, and etc. Many other authors used these approaches to study the vibration of laminated composite beams. For example, Rao et al. [2001] investigated the natural frequencies of a laminated simply supported beam. Friswell and Lees [2001] discussed the modes of vibration for nonhomogeneous damped beams composed of two materials with different stiffness, damping and mass properties. Li et al. [2008] studied the free vibration and buckling activities of laminated composite beams having lay-up in lateral direction subjected by axially loading. In general, the problems were solved by assuming that the variation of material properties was piecewise constants and continuity constraints were applied at the interface of two neighboring segments. As the number of segments increased, a large number of unknowns were generated and great computational efforts were needed.

Sheng and Wang [2018] investigated the nonlinear phenomena and resonant conditions of functionally graded (FG) beams when the beams were subjected to parametric and external excitations. They pointed out that, depending on the values of parameters, e.g., excitation frequency, excitation amplitude, damping, volume fraction exponent, etc., chaotic response could occur when the magnitude of excitation was greater than the Euler's buckling load. Kahya and Turan [2018] analyzed the free vibration and stability of FG sandwich beams without/with axial forces. Based on shear deformation theory, a finite element model was obtained to derive the natural frequency and buckling loads of FG sandwich beams. The effects of slenderness ratio and layer thickness to the fundamental frequency and buckling loads were examined. Lee and Lee [2017] studied the free vibration of FG beams by using transfer matrix method. They showed that when the slenderness ratio was not large, the effect produced by the coupling between the axial and bending displacements to the natural frequency of a beam shouldn't be ignored. Nevertheless, the coupling effect becomes tiny when the slenderness ratio is large.

Şimşek [2010], Şimşek and Kocatürk [2009], and Şimşek et al. [2012] employed Euler–Bernoulli beam theory combined with numerical integration to study the dynamics of a FG and an axially FG (AFG) beams with simply supported boundary condition, respectively. For the first two, they assumed that the variation of material properties of the beam was continuous in thickness direction and could be expressed by power-law functions. For the latter, the material properties were assumed to vary continuously in the axial direction. Their results showed that using FG/AFG beams had influential benefits to the dynamics of a beam-mass system.

Although stiffness-driven beam-like members with or without riding masses had been studied by many authors, generally, the mathematic model developed was able to be used for the scheme proposed in that study only. In other words, if the structure of the composite beam is changed, e.g., rearranging the assembly of composed materials/laminas, the mathematic model may have to be remodeled. Unlike other papers, in this study, the proposed model can be diversely applied on a composite beam having different arrangements and compositions of materials and layers. Meanwhile, by transversely applying specified arrays to form a periodic-array beam, the beam has the capability to shift its specific stiffness and frequency. This means that the embedded arrays can be treated as tuning parameters to the bending frequency of the beam. By assuming that all the layers of the periodic arrays are bonded, the periodicity and matching conditions across the interfaces arrays are taken into account by the Fourier series expansion. The dynamic characteristics induced by the inhomogeneity of materials/laminas of the proposed beam and the motion of the riding mass are examined.

2. Basic formulas

As shown in Figure 1 (top), a mass traveling on a finite simply supported periodic-array beam with rectangular cross-section having length ℓ, width W, and thickness H is considered. Here, the occurrence of delamination due to the interaction between laminas is prevented by the adjacent layers; hence, in the modeling, the arrays with bonded strips and layers are assumed. The Cartesian coordinate system xyz is on the inextensible centroidal axis of the beam ($y = 0$). Prior to the mass being set on motion, the beam is in straight and in the state of equilibrium. The composite beam is composed of a number of bonded periodic layers, basic and embedded laminas. The basic layer is a homogeneous lamina with the material c having the Young's modulus E_c and density ρ_c. The embedded lamina consists of periodic strips which are formed by two different rectangular strips of a and b of length ℓ; the Young's moduli and densities of the former and latter are E_a, E_b, ρ_a, and ρ_b, respectively. For the embedded lamina, the periodic arrangement is two strips of b separated by one strip of a; these strips are stacked in a row in the width (z) direction. For the beam, the periodic pattern is two basic layers separated by one embedded lamina and they are piled symmetrically in the thickness (y) direction. Hence, unless otherwise specified, the central ply of the embedded lamina is the strip a and the middle layer of the beam is the embedded lamina. By assuming that the beam is an inhomogeneous continuum, the two different strips of the embedded lamina and the two different layers of the beam are accounted for by spatial variation of the moduli of their phases. Therefore, the Young's modulus and density of the beam are biaxial periodic functions. It is known that the Fourier analysis can be applied in a limited range and will converge to that function in the interval. As a result, the variation of the moduli of the embedded lamina and the beam is expressed by the Fourier series expansion.

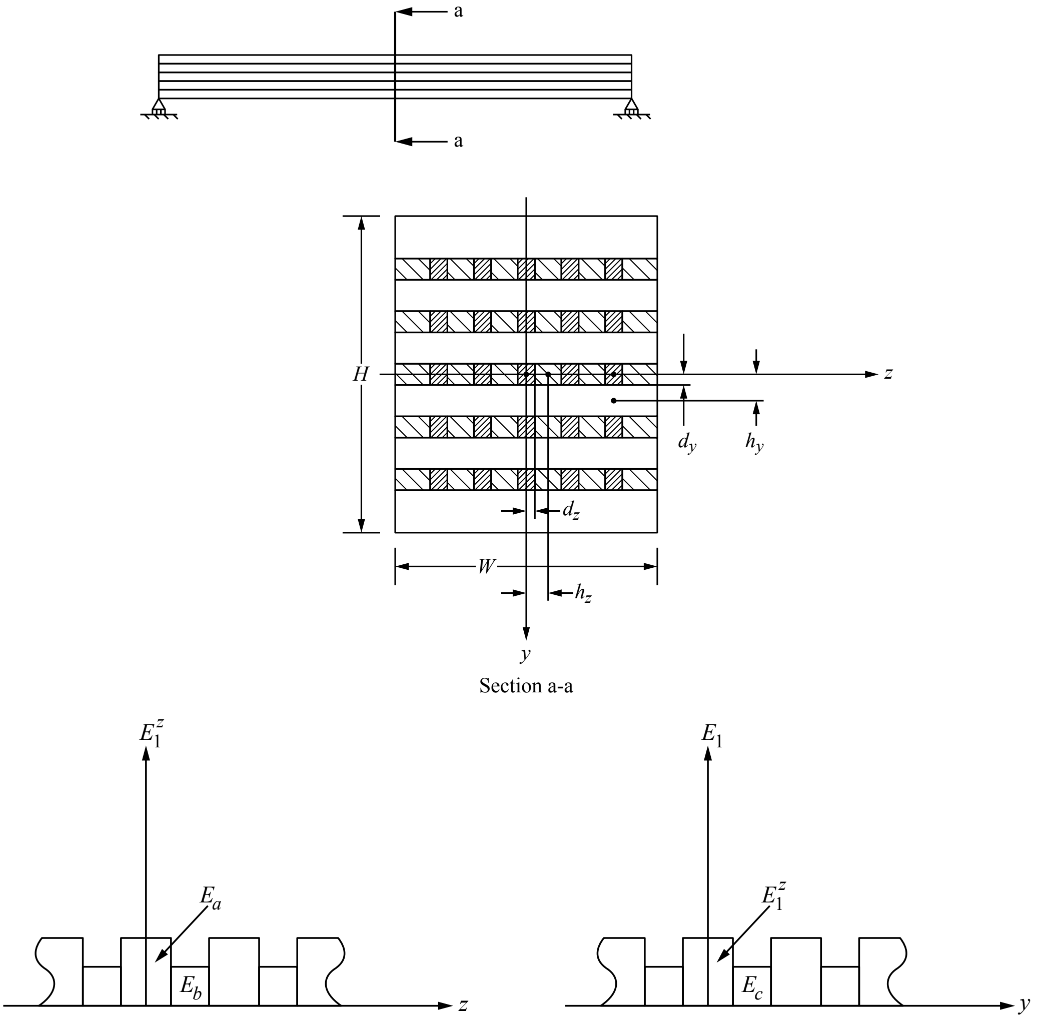

Figure 1. The schematic diagram of the cross-section of the periodic-array beam (top) and the Fourier series representation (bottom).

Due to symmetry, the variation of the moduli is assumed to be an even periodic function and is stated as a series of cosine terms; therefore, the number of strips and layers is odd. Referring to Figure 1 (bottom), let E_1^z, which is a periodic function in the z direction, be the axial Young's modulus of an embedded layer and be given by

$$\begin{aligned} E_1^z(z) &= E_a \frac{d_z}{h_z} + E_b\left(1 - \frac{d_z}{h_z}\right) + (E_a - E_b) \sum_{j=1}^{\infty} \frac{2}{j\pi} \sin\left(\frac{j\pi d_z}{h_z}\right) \cos\left(\frac{j\pi z}{h_z}\right) \\ &\equiv E_{10}^z + \sum_{j=1}^{\infty} E_{1j}^z \cos\left(\frac{j\pi z}{h_z}\right), \end{aligned} \tag{1a}$$

where

$$E_{1j}^{z}=\frac{2}{h_z}\int_0^{h_z}E_1^z(z)\cos\frac{j\pi z}{h_z}dz=(E_a-E_b)\frac{2}{j\pi}\sin\frac{j\pi d_z}{h_z}.$$

Here, d_z is one-half of the thickness of the strip a; h_z is one-half of the distance between the midpoint of two strips of b separated by one ply of a. Therefore, d_z/h_z presents the thickness ratio of the strip a that is present in one period $2h_z$ in the z (width) direction. Similarly, the axial Young's modulus of the beam $E_1(y,z)$ is also periodic in the y direction. Hence, one has

$$\begin{aligned}E_1(y,z)&=E_1^z\left(\frac{d_y}{h_y}\right)+E_c\left(1-\frac{d_y}{h_y}\right)+(E_1^z-E_c)\sum_{k=1}^{\infty}\frac{2}{k\pi}\sin\left(\frac{k\pi d_y}{h_y}\right)\cos\frac{k\pi y}{h_y}\\&\equiv E_{10}+\sum_{k=1}^{\infty}E_{1k}\cos\frac{k\pi y}{h_y},\end{aligned}\tag{1b}$$

where

$$E_{1k}=\frac{2}{h_y}\int_0^{h_y}E_1(y,z)\cos\frac{k\pi y}{h_y}dy=(E_1^z-E_c)\frac{2}{k\pi}\sin\frac{k\pi d_y}{h_y}.$$

Here, d_y is one-half of the thickness of an embedded lamina; h_y is one-half of the distance between the midpoint of two basic layers separated by one embedded lamina; d_y/h_y denotes the thickness ratio of an embedded lamina that is present in one period $2h_y$ in the y direction. Hence, there exist seven possible compositions of the composite beam:

(1) $0<d_z<h_z$ and $0<d_y<h_y$. The beam consists of embedded and basic laminas. The Young's moduli of the embedded lamina and the beam are given by (1a) and (1b).

(2) $d_z=0$ and $0<d_y<h_y$. The embedded layer reduces to a homogeneous lamina with the strip b. The axial Young's moduli of the embedded layer and the beam become, respectively,

$$E_1^z=E_b\quad\text{and}\quad E_1=E_1(y)=E_{10}+\sum_{k=1}^{\infty}E_{1k}\cos\frac{k\pi y}{h_y},\tag{1c}$$

where

$$E_{10}=E_b\left(\frac{d_y}{h_y}\right)+E_c\left(1-\frac{d_y}{h_y}\right)\quad\text{and}\quad E_{1k}=(E_b-E_c)\frac{2}{k\pi}\sin\left(\frac{k\pi d_y}{h_y}\right).$$

(3) $d_z=h_z$ and $0<d_y<h_y$. For this condition, one has

$$E_1^z=E_a\quad\text{and}\quad E_1=E_1(y)=E_{10}+\sum_{k=1}^{\infty}E_{1k}\cos\frac{k\pi y}{h_y},\tag{1d}$$

where

$$E_{10}=E_a\left(\frac{d_y}{h_y}\right)+E_c\left(1-\frac{d_y}{h_y}\right)\quad\text{and}\quad E_{1k}=(E_a-E_c)\frac{2}{k\pi}\sin\left(\frac{k\pi d_y}{h_y}\right).$$

(4) $d_y=0$. This means the vanish of embedded layers; the beam is homogeneous with the material c, i.e., $E_1=E_c$.

(5) $0 < d_z < h_z$ and $d_y = h_y$. The basic layer disappears; the beam is composed of two different kinds of vertical plies of the materials of a and b. The axial Young's modulus of the beam then turns into $E_1 = E_1(z) = E_1^z$ (1a).

(6) $d_z = 0$ and $d_y = h_y$. The beam becomes a homogeneous beam with the material b, i.e., $E_1 = E_b$.

(7) $d_z = h_z$ and $d_y = h_y$. The axial Young's modulus of the beam reduces to $E_1 = E_a$.

It is seen that the proposed model can be diversely used to simulate the composite beams having different arrangements of laminas and compositions of materials. Similar to the periodic distribution of Young's modulus, the density of the beam has the form

$$\rho(y,z) = \rho^z\left(\frac{d_y}{h_y}\right) + \rho_c\left(1 - \frac{d_y}{h_y}\right) + (\rho^z - \rho_c)\sum_{q=1}^{\infty}\frac{2}{q\pi}\sin\left(\frac{q\pi d_y}{h_y}\right)\cos\frac{q\pi y}{h_y} \equiv \rho_0 + \sum_{q=1}^{\infty}\rho_q\cos\frac{q\pi y}{h_y}, \quad (2)$$

where ρ^z is the density of an embedded lamina and is given by

$$\rho^z = \rho^z(z) = \rho_0^z + \sum_{p=1}^{\infty}\rho_p^z\cos\left(\frac{p\pi z}{h_z}\right),$$

with

$$\rho_0^z = \rho_a\frac{d_z}{h_z} + \rho_b\left(1 - \frac{d_z}{h_z}\right) \qquad \text{and} \qquad \rho_p^z = \frac{2}{h_z}\int_0^{h_z}\rho^z(z)\cos\frac{r\pi z}{h_z}dz = (\rho_a - \rho_b)\frac{2}{p\pi}\sin\frac{p\pi d_z}{h_z}.$$

Therefore, the mass per unit length of the beam can be obtained by

$$m = \int_{-W/2}^{W/2}\int_{-H/2}^{H/2}\rho(y,z)\,dy\,dz = m_0 + \sum_{p=1}^{\infty}m_p + \sum_{q=1}^{\infty}m_q + \sum_{p=1}^{\infty}\sum_{q=1}^{\infty}m_{pq} \equiv m_r(\hat{m}_0 + \hat{m}_{pq}), \quad (3)$$

where $m_r = \rho_r WH$, $r = c, b, a$. The selection of the subscript r depends on $\hat{d}_z$ and $\hat{d}_y$. For example, $r = c$ if cases (1)–(4) are considered; $r = b$ if cases (5) and (6) are taken into account; $r = a$ if case (7) is examined. Other parameters in (3) are given by

$$\hat{m}_0 = \left(\hat{\rho}_a\hat{d}_z + \hat{\rho}_b(1 - \hat{d}_z)\right)\hat{d}_y + \hat{\rho}_c(1 - \hat{d}_y),$$

with

$$\hat{\rho}_a = \frac{\rho_a}{\rho_r}, \quad \hat{\rho}_b = \frac{\rho_b}{\rho_r}(1 - \delta_{ra}), \quad \hat{\rho}_c = \frac{\rho_{cb}}{\rho_r}\delta_{rc}, \quad \hat{d}_z = \frac{d_z}{h_z}, \quad \hat{d}_y = \frac{d_y}{h_y},$$

$$
\begin{aligned}
\hat{m}_{pq} &= \sum_{p=1}^{\infty} \hat{m}_p + \sum_{q=1}^{\infty} \hat{m}_q + \sum_{p=1}^{\infty}\sum_{q=1}^{\infty} \hat{m}_{pq},\\
\hat{m}_p &= \frac{1}{2}\hat{d}_y \hat{h}_z \left[(\hat{\rho}_a - \hat{\rho}_b)\left(\frac{2}{p\pi}\right)^2 \sin(p\pi \hat{d}_z) \sin\frac{p\pi}{\hat{h}_z} \right], \quad \text{with } \hat{h}_z = \frac{2h_z}{W},\\
\hat{m}_q &= \frac{1}{2}\hat{h}_y \big[\big(\hat{\rho}_a \hat{d}_z + \hat{\rho}_b(1-\hat{d}_z)\big) - \hat{\rho}_c \big] \left(\frac{2}{q\pi}\right)^2 \sin(q\pi \hat{d}_y) \sin\frac{q\pi}{\hat{h}_y}, \quad \text{with } \hat{h}_y = \frac{2h_y}{H},\\
\hat{m}_{pq} &= \frac{1}{4}\hat{h}_z \hat{h}_y \left[(\hat{\rho}_a - \hat{\rho}_b)\left(\frac{2}{p\pi}\right)^2 \left(\frac{2}{q\pi}\right)^2 \sin\frac{p\pi}{\hat{h}_z} \sin(q\pi \hat{d}_y) \sin\frac{q\pi}{\hat{h}_y} \right],
\end{aligned}
$$

where $\hat{h}_z = 2h_z/W =$ the ratio of the distance of the period $2h_z$ to the width of the beam, $\hat{h}_y = 2h_y/H =$ the ratio of the length of the period $2h_y$ to the height of the beam, $\delta_{rp} =$ the Dirac delta symbol with $p = a, c$.

Since the axial Young's modulus of the beam is also spatial dependence, $E_1 = E_1(y, z)$, prior to deriving the equations of motion of the system, the resultant bending moment about the neutral axis of the cross section of the beam at time t has to be determined and is given by

$$
\widetilde{M} = \kappa \int_{-H/2}^{H/2} \int_{-W/2}^{W/2} E_1(y, z)\, y^2 dz\, dy, \tag{4a}
$$

where κ is the beam curvature; y is the perpendicular distance from the neutral axis to the centroid of the differential area dA, $dA = dy\, dz$. After some manipulations, it yields

$$
\widetilde{M} = \kappa I \left[E_{10} + \sum_{j=1}^{\infty} E_{1j} - \hat{I}_y \left(\sum_{k=1}^{\infty} E_{1k} + \sum_{j=1}^{\infty}\sum_{k=1}^{\infty} E_{1jk} \right) \right] \equiv \kappa E_r I \big(\hat{E}_{10} + \hat{E}_{1jk}^t \big), \tag{4b}
$$

where $I = \frac{1}{12}WH^3$, $\hat{I}_y = I_y/I = \frac{1}{8}(\hat{h}_y)^3$ with $I_y = \frac{1}{12}Wh_y^3$,

$$
\hat{E}_{10} = [\hat{E}_a \hat{d}_z + \hat{E}_b(1-\hat{d}_z)]\,\hat{d}_y + \hat{E}_c(1-\hat{d}_y), \qquad \text{with } \hat{E}_a = \frac{E_a}{E_r}, \quad \hat{E}_b = \frac{E_b}{E_r}(1-\delta_{ra}), \quad \hat{E}_c = \frac{E_c}{E_r}\delta_{rc},
$$

$$
\begin{aligned}
\hat{E}_{1jk}^t &= \sum_{j=1}^{\infty} \hat{E}_{1j} - \hat{I}_y \left(\sum_{k=1}^{\infty} \hat{E}_{1k} + \sum_{j=1}^{\infty}\sum_{k=1}^{\infty} \hat{E}_{1jk} \right),\\
\hat{E}_{1j} &= \frac{1}{2}\hat{d}_y \hat{h}_z \left[(\hat{E}_a - \hat{E}_b) \left(\frac{2}{j\pi}\right)^2 \sin(j\pi \hat{d}_z) \sin\frac{j\pi}{\hat{h}_z} \right],\\
\hat{E}_{1k} &= 6[\hat{E}_a \hat{d}_z + \hat{E}_b(1-\hat{d}_z) - \hat{E}_c] \left(\frac{2}{k\pi}\right)^4 \sin(k\pi \hat{d}_y) \sin\frac{k\pi}{\hat{h}_y},\\
\hat{E}_{1jk} &= 3\hat{h}_z \left[(\hat{E}_a - \hat{E}_b) \left(\frac{2}{j\pi}\right)^2 \left(\frac{2}{k\pi}\right)^4 \sin(j\pi \hat{d}_z) \sin\frac{j\pi}{\hat{h}_z} \sin(k\pi \hat{d}_y) \sin\frac{k\pi}{\hat{h}_y} \right].
\end{aligned}
$$

From (3) and (4b), one finds that increasing the number of layers decreases the distance of the period h_y. Therefore, when the beam has a many of layers, the length of h_y becomes a tiny value and the terms $\hat{h}_y$ and

$\hat{I}_y$ approach to zero such that $\hat{m}_{pq} \to \sum_{p=1}^{\infty} \hat{m}_p$ and $\hat{E}^t_{1jk} \to \sum_{j=1}^{\infty} \hat{E}_{1j}$. This means that as h_y decreases, the Young's modulus and mass of the composite beam converge to $E_{10} + \sum_{j=1}^{\infty} E_{1j}$ and $m_0 + \sum_{p=1}^{\infty} m_p$, respectively. Similar phenomenon is also observed when h_z and $\hat{h}_z$ are taken into account.

As mentioned previously, the number of strips and layers is always odd. The distance of the periods h_z and h_y along the width and height can be calculated and yields

$$h_z = \frac{W}{2i \pm 2\hat{d}_z}, \quad 0 < \hat{d}_z < 1, \quad i = 2, 3, 4, \dots, \tag{5a}$$

$$h_y = \frac{H}{2j \pm 2\hat{d}_y}, \quad 0 < \hat{d}_y < 1, \quad j = 2, 3, 4, \dots, \tag{5b}$$

where i and j are the number of the strips b and the total of basic layers, respectively. The plus and minus signs used in (5a) are when the number of the strips b is less than and greater than the total of the strips a, respectively. Therefore, for the plus and minus signs, the number of strips of an embedded lamina is equal to $5 + 4(i - 1)$ and $3 + 4(i - 1)$, $i = 1, 2, 3, \dots$, respectively. The selection of the plus and minus signs in (5b) can be done similarly. For example, a sandwich (three horizontal layers) beam is composed of one embedded lamina (core) and two basic layers. The embedded lamina consists of three strips of a of equal lateral thickness $2d_z$ and four strips of b of equal lateral thickness $2(h_z - d_z)$. The lengths of h_z and h_y are given by $h_z = W/(8 - 2\hat{d}_z)$, $0 < \hat{d}_z < 1$, and $h_z = H/(4 - 2\hat{d}_y)$, $0 < \hat{d}_y < 1$, respectively. Another example is that a composite beam consists of five horizontal layers, three embedded and two basic laminas. The period h_y then is $h_y = H/(4 + 2\hat{d}_y)$. Note that (5a) and (5b) are not applied to the cases when $\hat{d}_z = 0$, 1 and $\hat{d}_y = 0$, 1, respectively. For $\hat{d}_z = 0$ and 1, the embedded lamina reduces to a homogeneous layer having the materials b and a, respectively. For $\hat{d}_y = 0$ and 1, the beam is homogeneous having the material c and the beam consists of two different vertical layers of a and b, respectively.

As the structure of the composite beam is established, in the following, the dynamics of a beam-mass system is considered. From Figure 2, the mechanics of the interface between the mass and beam is determined by modeling the mass as a rigid body that is rolling on the beam. The equations governing the motion of the system can be derived from the dynamic equilibrium of forces and momenta and are given by

$$\boldsymbol{F}_{,s} + \boldsymbol{f} = m_r(\hat{m}_0 + \hat{m}_{pq})\, \boldsymbol{r}_{,tt}, \quad 0 < s < l,\ t > 0, \tag{6a}$$

$$\boldsymbol{F} = T\hat{\boldsymbol{\tau}} + V\boldsymbol{n} = (T\cos\theta - V\sin\theta)\, \boldsymbol{i} + (T\sin\theta + V\cos\theta)\, \boldsymbol{j}, \tag{6b}$$

$$E_r(\hat{E}_{10} + \hat{E}^t_{1jk})\, I v_{,sss} + V = 0, \tag{6c}$$

with the inextensibility constraint $\boldsymbol{r}_{,s} \cdot \boldsymbol{r}_{,s} = 1$. The corresponding boundary conditions for the simply supported beam are

$$u(0, t) = v(0, t) = v(\ell, t) = \frac{\partial^2 v(0, t)}{\partial s^2} = \frac{\partial^2 v(\ell, t)}{\partial s^2} = 0, \tag{7a}$$

$$T(\ell, t)(1 + u_{,s}) + E_r(\hat{E}_{10} + \hat{E}^t_{1jk}) I v_{,sss}\, v_{,s} = 0, \quad \text{at } s = \ell, \tag{7b}$$

where (7b) is obtained when the resultant force in the $\boldsymbol{i}$ direction vanishes at $s = \ell$. In above equations, $\boldsymbol{i}$, $\boldsymbol{j}$ = the unit vectors in the horizontal and gravitational (transverse) directions, respectively, $\boldsymbol{r}(s, t) =$

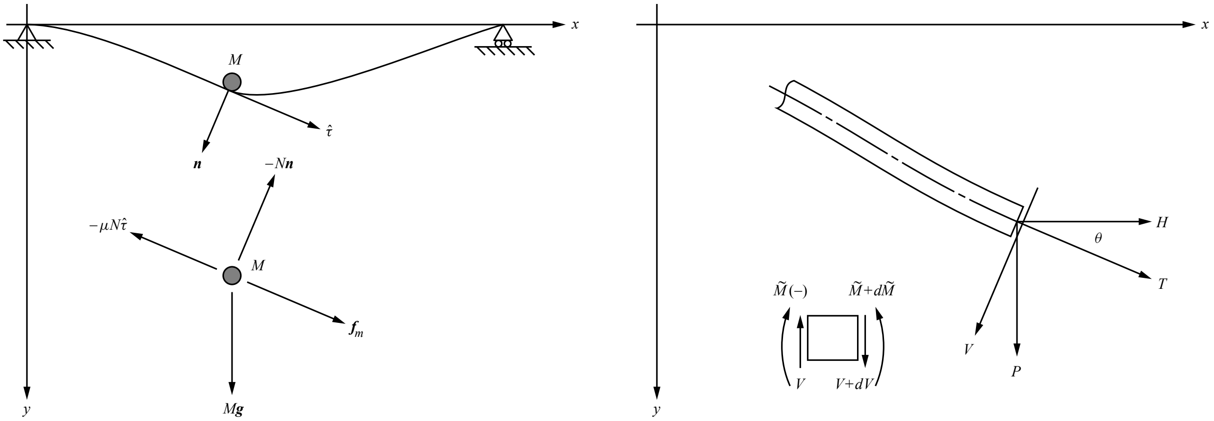

Figure 2. System configuration (left) and force equilibrium diagram (right).

$[x(s)+u(s,t)]\boldsymbol{i}+v(s,t)\boldsymbol{j}$ with $u(s,t)$ and $v(s,t)$ being the axial and transverse displacements of the beam measured from the undeformed state, respectively, $\boldsymbol{n}$, $\hat{\boldsymbol{\tau}}$ = the unit normal and tangent vectors to the beam configuration, respectively, T, V, θ = the axial and transverse forces in the beam and the angle between the neutral axis of the beam and the x-axis, respectively. The subscripts s and t mean the s and t differentiation. In this study, the slenderness ratio of the beam $s=\ell(\sqrt{I/A})^{-1}$ [Han et al. 1999] selected is a large value such that the Euler–Bernoulli beam theory is applicable to be applied, where A is the cross-sectional area of the beam. By considering the small deformation theory and applying the inextensibility constraint $\boldsymbol{r}_{,s}\cdot\boldsymbol{r}_{,s}=1$, the axial displacement of the beam is in the second order nonlinearity and can be neglected. Therefore, $\boldsymbol{r}(s,t)=x(s)\boldsymbol{i}+v(s,t)\boldsymbol{j}$ and $\hat{\tau}=\boldsymbol{i}+v_{,s}\boldsymbol{j}$. The force $\boldsymbol{f}$ represents the external forces including the weight and the reactions of the moving mass upon the composite beam and can be expressed as

$$\boldsymbol{f}=(N\boldsymbol{n}+\mu N\hat{\boldsymbol{\tau}})\,\bar{\delta}\big(s-\bar{s}(t)\big), \tag{8}$$

where N, μ, $\bar{\delta}[s-\bar{s}(t)]$, and $\bar{s}(t)$ represent the dynamic interaction force between the mass and beam, coefficient of friction, Dirac delta function, and the position of mass along the arc of the beam at time t, respectively. The equation of motion of the moving mass is given by (Figure 2)

$$M\boldsymbol{a}_M=M\frac{d^2}{dt^2}\big[\boldsymbol{r}\big(\bar{s}(t),t\big)\big]=M[\boldsymbol{r}_{,ss}(\bar{s}_{,t})^2+2\boldsymbol{r}_{,st}\,\bar{s}_{,t}+\boldsymbol{r}_{,s}\,\bar{s}_{,tt}+\boldsymbol{r}_{,tt}]=M\boldsymbol{g}+\boldsymbol{f}_{\hat{\tau}}-\mu N\hat{\boldsymbol{\tau}}-N\boldsymbol{n}, \tag{9}$$

where $\boldsymbol{a}_M$ = the acceleration of the mass, M = total mass of the moving mass, $\boldsymbol{g}=g\boldsymbol{j}$, $\boldsymbol{f}_{\hat{\tau}}=Mf\hat{\boldsymbol{\tau}}=Mf(\boldsymbol{i}+v_{,s}\boldsymbol{j})$ = tangential propelling thrust with f being a prescribed function of time. Hence, loss of contact occurs if the interaction force becomes zero. The force N can be obtained by taking the inner product of (9) with $\boldsymbol{n}$ and is given by

$$N=[M\boldsymbol{g}-M\boldsymbol{a}_M]\cdot\boldsymbol{n}|_{s=\bar{s}(t)}. \tag{10}$$

To determine the axial force T, one substitutes (6b), (6c), and (8)–(10) into (6a) and assumes that the variation of axial force remains continuous at the mass. The axial force T can be obtained by taking the inner product of (6a) by the unit vector $\boldsymbol{i}$ and integrating it from 0 to $s=\bar{s}(t)$ and $s=\bar{s}(t)$ to ℓ and using (7b). Inserting this result into (6a) in the $\boldsymbol{j}$ direction and neglecting nonlinear terms when compare these terms to the linear term of $v(s,t)$ and unity, the equation of motion of the nonhomogeneous beam with a riding mass is given by

$$m_r(\hat{m}_0+\hat{m}_{pq})\,v_{,tt}+E_rI(\hat{E}_{10}+\hat{E}^t_{1jk})\,v_{,ssss}+\boldsymbol{f}\cdot\boldsymbol{j}=0,\quad 0<s<\ell,\ t>0. \tag{11}$$

The differential equation is linear in the displacement field. Let the variable $v(s,t)$ be of the form

$$v(s,t)=\sum_{j=1}^{n}\tilde{q}_j(s)\,\tilde{h}_j(t)\equiv\tilde{\boldsymbol{q}}(s)^T\,\tilde{\boldsymbol{h}}(t), \tag{12}$$

where $\tilde{\boldsymbol{h}}(t)$ is the time dependent vector to be determined; n is a suitably large number to assure convergence. In order that the variable $v(s,t)$ satisfies the boundary condition given by (7a), one represents $\tilde{\boldsymbol{q}}(s)$ as a vector of a continuous function:

$$\tilde{\boldsymbol{q}}(s)=\left(\sin\frac{\pi s}{\ell},\sin\frac{2\pi s}{\ell},\ldots,\sin\frac{i\pi s}{\ell},\ldots,\sin\frac{n\pi s}{\ell}\right)^T,\quad 0<s<\ell, \tag{13}$$

which satisfies the spatial boundary constraints $\tilde{\boldsymbol{q}}|_{s=0,\ell}=\frac{\mathrm{d}^2\tilde{\boldsymbol{q}}}{\mathrm{d}s^2}|_{s=0,\ell}=\boldsymbol{0}$.

To obtain the normalized equations of motion of the combined system, one substitutes (8)–(10), (12), and (13) into (11) and introduces the following nondimensional quantities:

$$\tau=\sqrt{\frac{E_rI}{m_r\ell^4}}\,t,\quad \hat{M}=\frac{M}{m_r\ell},\quad \hat{N}=\frac{m_r\ell^3}{ME_rI}N,\quad \hat{f}=\frac{m_r\ell^3}{E_rI}f,\quad \hat{g}=\frac{m_r\ell^3}{E_rI}g,\quad \eta=\frac{s}{\ell},\quad \xi=\frac{\bar{s}}{\ell}. \tag{14}$$

To eliminate spatial dependence of (11), the Galerkin's procedure is employed and is done by multiplying (11) by the weighting vector $\boldsymbol{q}(\eta)$ and integrating (11) w.r.t. to η from 0 to 1. The result yields

$$\begin{aligned}\left(\boldsymbol{I}+\frac{2\hat{M}}{\hat{m}_0+\hat{m}_{pq}}\boldsymbol{G}_1\right)\ddot{\boldsymbol{h}}+\frac{4\hat{M}}{\hat{m}_0+\hat{m}_{pq}}\dot{\xi}\boldsymbol{G}_2\dot{\boldsymbol{h}}+\left[\frac{\hat{E}_{10}+\hat{E}^t_{1jk}}{\hat{m}_0+\hat{m}_{pq}}\boldsymbol{\Omega}^2_h+\frac{2\hat{M}}{\hat{m}_0+\hat{m}_{pq}}(-\hat{f}\boldsymbol{G}_2-\dot{\xi}^2\boldsymbol{G}_3)\right]\boldsymbol{h}&\\ +\frac{2\hat{M}}{\hat{m}_0+\hat{m}_{pq}}\ddot{\xi}\boldsymbol{G}_2\boldsymbol{h}=\frac{2\hat{M}\hat{g}}{\hat{m}_0+\hat{m}_{pq}}\boldsymbol{s}_\xi,\quad 0<\xi<1,\ \tau>0,&\end{aligned} \tag{15a}$$

where the superposed prime and dot denoting the η and τ differentiation, $\boldsymbol{I}=n\times n$ unit matrix, $\boldsymbol{q}=\boldsymbol{q}(\eta)$, $\boldsymbol{h}=\boldsymbol{h}(\tau)$, $\boldsymbol{s}_\xi=s_{\xi j}$ with $s_{\xi j}=\sin j\pi\xi$ when $j=1,2,\ldots,n$; $\boldsymbol{G}_1=\int_0^1\delta(\eta-\xi)\boldsymbol{q}\boldsymbol{q}^Td\eta$, $\boldsymbol{G}_2=\int_0^1\delta(\eta-\xi)\boldsymbol{q}\boldsymbol{q}'^Td\eta$, $\boldsymbol{G}_3=\int_0^1\delta(\eta-\xi)\boldsymbol{q}\boldsymbol{q}''^Td\eta$, $\boldsymbol{\Omega}^2_h=2\int_0^1\boldsymbol{q}\boldsymbol{q}''''^Td\eta=\mathrm{diag}[(\omega^h_j)^2]$ with $\omega^h_j=(j\pi)^2$ being the normalized frequency of the j-th mode vibration of the homogeneous beam. Equations (9) and (10) become

$$\ddot{\xi}-\mu\boldsymbol{q}''^T\boldsymbol{h}(\dot{\xi})^2-2\mu\boldsymbol{q}'^T\dot{\boldsymbol{h}}\dot{\xi}-\mu\boldsymbol{q}^T\ddot{\boldsymbol{h}}-\hat{g}\boldsymbol{q}'^T\boldsymbol{h}=\hat{f}-\mu\hat{g},\quad \eta=\xi,\ \tau>0, \tag{15b}$$

$$\hat{N}=\hat{g}-[\boldsymbol{q}^T\ddot{\boldsymbol{h}}_1-2\boldsymbol{q}'^T\dot{\boldsymbol{h}}_1\dot{\xi}-\boldsymbol{q}''^T\boldsymbol{h}_1\dot{\xi}^2],\quad \eta=\xi,\ \tau>0. \tag{15c}$$

The initial conditions are

$$\dot{\xi}(0)=\dot{\xi}_0,\quad \xi(0)=\xi_0,\quad \boldsymbol{h}(0)=\dot{\boldsymbol{h}}(0)=\boldsymbol{0}, \tag{16}$$

where $\mathbf{0}$ is $n \times 1$ zero vector; $\dot{\xi}_0$ and ξ_0 are the initial speed and the initial position of mass on the beam, respectively. As shown in (15a), by properly arranging the material and geometric properties of periodic arrays, the beam frequency is able to be varied. In other words, the proposed beam has the potential to change its natural frequency to avoid the growth of small amplitude vibration and the occurrence of resonance. It is mentioned here that (15b) was obtained by eliminating the normal reaction force N of the beam on the mass between the two equations in directions $\boldsymbol{i}$ and $\boldsymbol{j}$ of (9).

After the mass left the beam, the dynamics of the system becomes the free vibration of the nonhomogeneous beam with nonzero initial conditions. In this situation, (15b) and (15c) vanish and (15a) reduces to

$$\ddot{\boldsymbol{h}} + \frac{\hat{E}_{10} + \hat{E}^t_{1jk}}{\hat{m}_0 + \hat{m}_{pq}} \boldsymbol{\Omega}^2_h \boldsymbol{h} = \mathbf{0}, \qquad \tau > \tau|_{\xi=1}, \tag{17a}$$

with the initial conditions

$$\boldsymbol{h}(0) = \boldsymbol{h}(\tau|_{\xi=1}) \quad \text{and} \quad \dot{\boldsymbol{h}}(0) = \dot{\boldsymbol{h}}(\tau|_{\xi=1}), \tag{17b}$$

where $\boldsymbol{h}(\tau|_{\xi=1})$ and $\dot{\boldsymbol{h}}(\tau|_{\xi=1})$ denote the amplitude and velocity of response of the beam when the mass is at the right end.

To verify the existence of solution of the system, a new state vector z is introduced into (15a) and (15b) to form the integrational scheme. Let $z = (\dot{\boldsymbol{h}}^T, \dot{\xi}, \boldsymbol{h}^T, \xi)^T$ be a $2n+2$ vector with the associated initial condition $z(0) = (\mathbf{0}^T, \dot{\xi}_0, \mathbf{0}^T, 0)^T$. The two equations can be written as

$$\boldsymbol{A}\dot{z} + \boldsymbol{B}z + \boldsymbol{p} = \mathbf{0}. \tag{18}$$

In (18), $\boldsymbol{A}$ and $\boldsymbol{B}$ are $(2n+2) \times (2n+2)$ matrices and $\boldsymbol{p}$ is the $(2n+2)$ vector defined by

$$\boldsymbol{A} = \begin{bmatrix} [\boldsymbol{I} + \frac{2\hat{M}}{\hat{m}_0+\hat{m}_{pq}} \boldsymbol{G}_1] & \frac{2\hat{M}}{\hat{m}_0+\hat{m}_{pq}} (\boldsymbol{G}_2 \boldsymbol{h}) & [\mathbf{0}] & \mathbf{0} \\ -\mu \boldsymbol{q}^T & 1 & \mathbf{0}^T & 0 \\ [\mathbf{0}] & \mathbf{0} & \boldsymbol{I} & \mathbf{0} \\ \mathbf{0}^T & 0 & \mathbf{0}^T & 1 \end{bmatrix},$$

$$\boldsymbol{B} = \begin{bmatrix} [\frac{4\hat{M}}{\hat{m}_0+\hat{m}_{pq}} \dot{\xi} \boldsymbol{G}_2] & \mathbf{0} & [\frac{\hat{E}_{10}+\hat{E}^t_{1jk}}{\hat{m}_0+\hat{m}_{pq}} \boldsymbol{\Omega}^2_h + \frac{2\hat{M}}{\hat{m}_0+\hat{m}_{pq}} (-\bar{f} \boldsymbol{G}_2 + \dot{\xi}^2 \boldsymbol{G}_3)] & \mathbf{0} \\ \mathbf{0}^T & -\mu(\dot{\xi} \boldsymbol{q}''^T \boldsymbol{h} + 2\boldsymbol{q}'T \dot{\boldsymbol{h}}) & -\hat{g} \boldsymbol{q}'^T & 0 \\ -\boldsymbol{I} & \mathbf{0} & [\mathbf{0}] & \mathbf{0} \\ \mathbf{0}^T & -1 & \mathbf{0}^T & 0 \end{bmatrix},$$

$$\boldsymbol{p} = \left(-\frac{2\hat{M}\hat{g}}{\hat{m}_0 + \hat{m}_{pq}} \boldsymbol{s}^T_{\xi,} - (\hat{f} - \mu \hat{g}), \mathbf{0}^T, 0 \right)^T,$$

where $\boldsymbol{A}$ is a nonsingular matrix and $[\mathbf{0}]$ is a $n \times n$ zero matrix.

3. Numerical results and discussions

Numerical results refer to an assumed model wherein a mass travels with variable speed on a finite simply supported beam having transversely periodic arrays. To study the influence produced by the variation of various parameters to the dynamics of the system, the Runge–Kutta method with sixth order accuracy

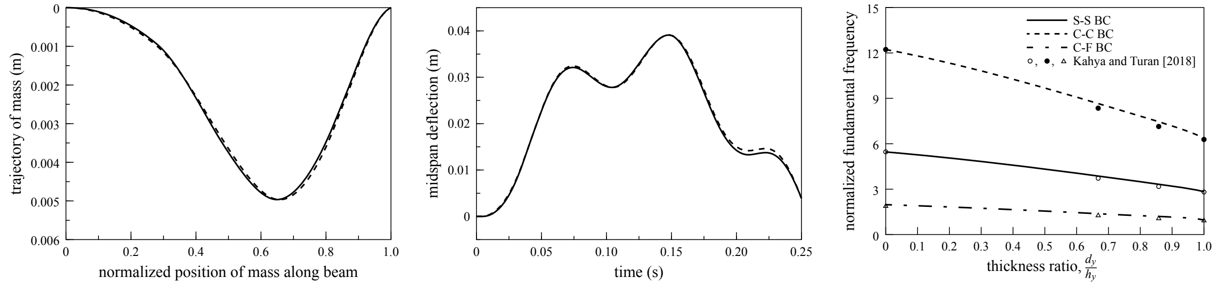

Figure 3. Comparison of the results with those reported in [Mohebpour et al. 2016] (dashed line, left), [Tao et al. 2016] (dashed line, middle), and [Kahya and Turan 2018] (symbolized by point symbols ○, •, and Δ, right).

is employed to numerically integrate (18). The number of terms of the Fourier series in (1) and (2) is set to be 30 to assure convergence. The convergence of the model is tested by increasing the terms of approximation. It shows that for $n \geq 10$, the difference among the results is negligible. Hence, the dimension n of z is set to be 15 to retain for sufficient accuracy.

To validate the accuracy of the model, in agreement with previous works is considered. As shown in Figure 3, the accuracy of the model is verified by numerically integrating (18) and then the solutions (solid lines) of this study are compared with the results (dashed lines) reported in Figure 3 by Mohebpour et al. [2016] and in the Figure 2 by Tao et al. [2016]. The parameters selected are the same as those used in the two papers, respectively, and are given in Table 1. Note that in [Tao et al. 2016], the massless point force was used; under such condition, (18) reduces to $\dot{\boldsymbol{z}} + \boldsymbol{B}\boldsymbol{z} + \boldsymbol{p} = \boldsymbol{0}$, where

$$\boldsymbol{z} = (\dot{\boldsymbol{h}}^T, \boldsymbol{h}^T)^T, \quad \boldsymbol{B} = \begin{bmatrix} [\boldsymbol{0}] & [\frac{\hat{E}_{10}+\hat{E}^t_{1jk}}{\hat{m}_0+\hat{m}_{pq}}\,\boldsymbol{\Omega}^2_h] \\ -\boldsymbol{I} & [\boldsymbol{0}] \end{bmatrix}, \quad \boldsymbol{p} = \left(-\frac{2\hat{P}}{\hat{m}_0+\hat{m}_{pq}}\,\boldsymbol{s}^T_\xi, \boldsymbol{0}^T\right)^T, \quad \text{and} \quad \hat{P} = \frac{\ell^2}{E_r I}P,$$

with P being the massless point force. As shown in Figure 3 (left and middle), the solutions derived from the proposed model nearly coincide with the results obtained by Mohebpour et al. [2016] and Tao et al. [2016].

In addition to the verification mentioned above, the normalized fundamental frequency ($\equiv \omega_1$) of the proposed beam under simply-supported boundary condition is checked and compares it with the first nondimensional frequency ($\equiv \varpi_1$) reported in the Table 3 by [Kahya and Turan 2018]. The relation

[Mohebpour et al. 2016]	Stiffness $E = 2020.797216 \cdot 10^8$ Pa, density $\rho = 15267.2\,\mathrm{kg/m^3}$, length $\ell = 4.352$ m, thickness $H = 0.072322$ m, width $W = 0.018113$ m Mass of the traveling mass $m = 21.8$ kg, mass speed $v = 27.49$ m/s
[Tao et al. 2016]	Stiffness $E = 72.4$ GPa, density $\rho = 2770\,\mathrm{kg/m^3}$, length $\ell = 10$ m, thickness $H = 0.5$ m, width $W = 0.4$ m Magnitude of the point force $P = 500$ kN, force speed $v = 40$ m/s

Table 1. The properties of the beams and moving masses used in [Mohebpour et al. 2016] and [Tao et al. 2016].

$k = 0$	$\hat{d}_y = 0$ (a homogeneous ceramic beam)
$k = 1$	$\hat{d}_y = 0.67$ ($d_y = 0.5t_m$ and $h_y = 0.75t_m = 1.5t_c$), t_c, t_m = the thickness of one ceramic lamina and metal core, respectively
$k = 2$	$\hat{d}_y = 0.857$ ($d_y = 0.5t_m$ and $h_y = 0.583t_m = 3.5t_c$)
$k = 10$	$\hat{d}_y \approx 1$ (a beam with almost all metal material)

Table 2. The relations between k and the parameters used in Figure 3 (right).

Set 1	The Young's moduli (GPa) of the strips of a, b, and the material c of the basic layer $E_a = 205$ ($\hat{E}_a = 2.05$), $E_b = 142$ ($\hat{E}_b = 1.42$), $E_c = 100$ ($\hat{E}_c = 1$) The densities (10^3 kg/m^3) of the strips of a, b, and the material c of the basic layer $\rho_a = 7.7$ ($\hat{\rho}_a = 1.1$), $\rho_b = 1.6$ ($\hat{\rho}_b = 0.229$), $\rho_c = 7$ ($\hat{\rho}_c = 1$)
Set 2	$E_a = 250$ ($\hat{E}_a = 2.5$), $E_b = 175$ ($\hat{E}_b = 1.75$), $E_c = 100$ ($\hat{E}_c = 1$) $\rho_a = 3.5$ ($\hat{\rho}_a = 0.5$), $\rho_b = 5.25$ ($\hat{\rho}_b = 0.75$), $\rho_c = 7$ ($\hat{\rho}_c = 1$)

Table 3. The material properties of the proposed beam for set 1 and set 2.

between these two frequencies ϖ_1 and ω_1 is $\varpi = (\ell/Hs)\omega_1$, where s denotes the slenderness ratio s. For a beam having rectangular cross-section area with height H, the slenderness ratio s equals $\sqrt{12}\,\ell/H$ and hence

$$\varpi_1 = \frac{\omega_1^h}{\sqrt{12}} \sqrt{\frac{\hat{E}_{10} + \hat{E}^t_{1jk}}{\hat{m}_0 + \hat{m}_{pq}}}.$$

Therefore, with the same materials as those used in [Kahya and Turan 2018], the frequency ω_1 varies from 2.849 ($\varpi_1 = 2.8057$), where $\omega_1 = \omega_1^h/\sqrt{12} = 2.849$ ($\omega_1^h = \pi^2$, [Han et al. 1999]), to 5.483 ($\varpi_1 = 5.4658$). The frequency of the proposed beam under other kinds of boundary conditions can be obtained by similar ways. For example, the frequency ω_1 for clamped-clamped BC is from 6.458 ($\varpi_1 = 6.302$), where $6.458 = \omega_1 = \omega_1^h/\sqrt{12}$ ($\omega_1^h = (4.73)^2$, [Han et al. 1999]), to 12.42 ($\varpi_1 = 12.235$). Figure 3 (right) shows the frequency ω_1 of the proposed beam versus the thickness ratio $\hat{d}_y$ under different boundary conditions and the results reported in the Table 3 by [Kahya and Turan 2018] (symbolized by point symbols $\bigcirc$, $\bullet$, and Δ) where the face-core-face thickness ratio 1-0-1 is chosen and the power-law exponent k selected are $k = 0$, 1, 2, and 10. In this figure, the FG beam is modeled as a sandwich beam composed of one metal core and two ceramic face layers. The solid, dashed, and central lines shown denote the results of this study under the simply-supported, clamped-clamped, and clamped-free boundary conditions, respectively. The relation between the power-law exponent k and the parameters used in Figure 3 (right) is given in Table 2. It clearly indicates that the solutions derived from the proposed model are in agreement with the results obtained by Kahya and Turan [2018].

To parametric study the dynamics of a mass traveling on the periodic-array beam, two sets of parameters are chosen and given in Table 3. The difference between the two sets is different arrangements of material properties. The numerical order of the Young's moduli and densities of materials selected in set 1 and set 2 is $E_a > E_b > E_c$, $\rho_a > \rho_c > \rho_b$ and $E_a > E_b > E_c$, $\rho_c > \rho_b > \rho_a$, respectively.

The geometric properties of the beam are: $\ell = 10\,\mathrm{m}$ and $W = H = 0.15\,\mathrm{m}$, where the slenderness ratio $s = \ell(\sqrt{I/A})^{-1} = \sqrt{12}\,\ell/H = 231$. The traveling mass has the mass $M = 200\,\mathrm{kg}$. Note that in the following figures, unless otherwise specified, the dashed line without symbol denotes the beam is a homogeneous beam having the material c. Meanwhile, in Figures 4–8, the mass moves at constant speed $\dot{s}(t) = 20\,\mathrm{m/s}$. With the view to illustrating the diversity of the proposed model, firstly the dynamics of a sandwich beam (having three horizontal layers) with a riding mass is considered and presented in Figures 4 and 5; the parameter set 1 is chosen. The beam consists of one embedded and two basic laminas; the core layer consists of three and two strips of a and b, respectively. The h_z and h_y are given by $h_z = 0.15/(4+2\hat{d}_z)$, $0 < \hat{d}_z < 1$, and $h_y = 0.15/(4-2\hat{d}_y)$, $0 < \hat{d}_y < 1$.

Figure 4 presents the trajectory of mass (mm) versus the position of mass along the beam (m) and the time history (s) of the midpoint deflection (mm) of the beam, respectively. The thickness ratios $\hat{d}_y$ and $\hat{d}_z$ are $\hat{d}_y = 0.25$ and $\hat{d}_z = 0.1$ (symbolized by $+$), 0.5 (symbolized by $\square$), and 0.9 (symbolized by Δ). Figure 5 presents similar information to that shown in Figure 4, except $\hat{d}_z = 0.25$ and three different values of $\hat{d}_y$ being selected, $\hat{d}_y = 0.1$ (symbolized by $+$), 0.5 (symbolized by $\square$), and 0.9 (symbolized by Δ). These two figures clearly indicate that different arrangements of the geometric and material properties of the arrays bring different capabilities of the beam to reduce the amplitude of vibration, even after the mass left the terminal point. Figure 4 also indicates that the strip a having the largest density, increasing $\hat{d}_z$ increases not only the stiffness but also the mass of the embedded lamina; this causes that changing $\hat{d}_z$ makes a little difference to reduce the amplitude of beam vibration. For the thickness ratio $\hat{d}_y$, since the embedded layer has greater specific stiffness than the basic layer, as shown in Figure 5, increasing $\hat{d}_y$ has significant potentials to diminish the vibration of the system.

To study the impact arising from different arrangements of the moduli of the arrays, in Figure 6, the midpoint deflection of the beam (mm) is plotted as a function of the variation of $\hat{d}_z$ (Figure 6, left) and $\hat{d}_y$ (Figure 6, right) when the mass reaches the midpoint ($\xi = 0.5$). The parameter set 1 and the beam having horizontally three embedded and four basic laminas are chosen. The embedded layer consists of three and four strips of a and b, respectively. The periods h_z and h_y are $h_z = 0.15/(8-2\hat{d}_z)$ $(0 < \hat{d}_z < 1)$ and $h_y = 0.15/(8-2\hat{d}_y)$ $(0 < \hat{d}_y < 1)$. In Figure 6 (left), $\hat{d}_y$ selected are: 0 (dashed line, case (4)), 0.1 (symbolized by $+$), 0.25 (symbolized by $\square$), 0.5 (symbolized by Δ), 0.75 (symbolized by $\bigcirc$), and 1 (symbolized by $\oplus$, cases (5, 6, 7)). In Figure 6 (right), $\hat{d}_z$ used are: 0 (without symbol), 0.1 (symbolized by $+$, cases (2, 6)), 0.25 (symbolized by $\square$), 0.5 (symbolized by Δ), 0.75 (symbolized by $\bigcirc$), and 1.0 (symbolized by $\oplus$, cases (3, 7)). This figure clearly shows that if the embedded lamina has higher specific stiffness than the basic layer, the integration of embedded laminas into the beam increases the capability of the beam to diminish the vibration caused by the motion of riding mass. However, in set 1, the strips of a and b have the largest and lowest densities, respectively. Hence, when $\hat{d}_z$ increases from 0 to 1, the Young's modulus ratio is from $\hat{E}_b = 1.42$ to $\hat{E}_a = 2.05$ and the density ratio is from $\hat{\rho}_b = 0.229$ to $\hat{\rho}_a = 1.1$. In other words, the increase of $\hat{d}_y$ and $\hat{d}_z$ increases not only the stiffness but also the mass of the beam. This implies when $\hat{d}_y$ becomes large, the increase of density becomes greater than that of the Young's modulus such that greater $\hat{d}_z$ has lower potential to reduce the vibration than smaller $\hat{d}_z$.

In order to fully understand the influence produced by the change of the beam properties, the set 2 ($E_a > E_b > E_c$ and $\rho_c > \rho_b > \rho_a$) is chosen. The speed and mass of the moving mass are the same as before. Figure 7 presents similar information to that shown in Figure 6. This figure indicates that when

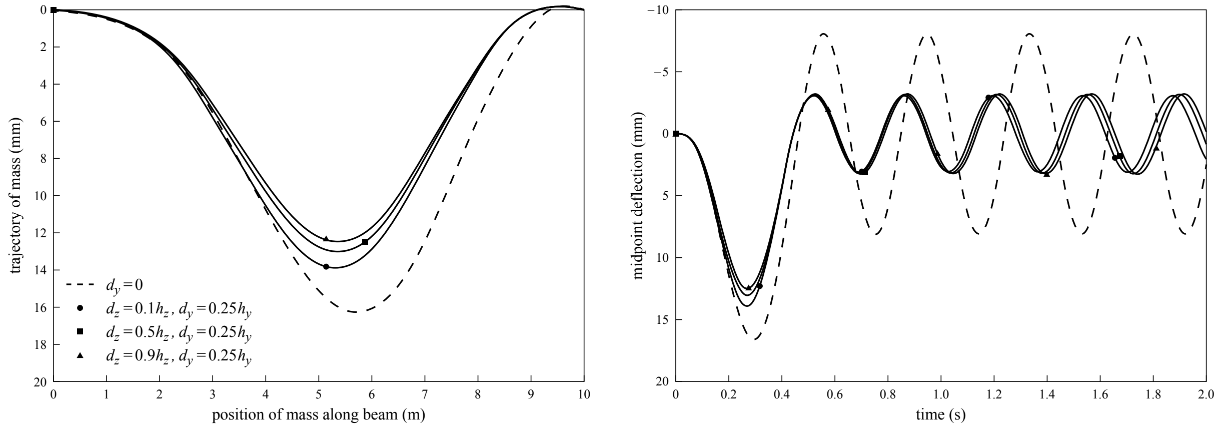

Figure 4. Trajectory of mass (mm) versus the position of mass along the beam (m) (left) and the time history (s) of the midpoint deflection (mm) of the beam (right).

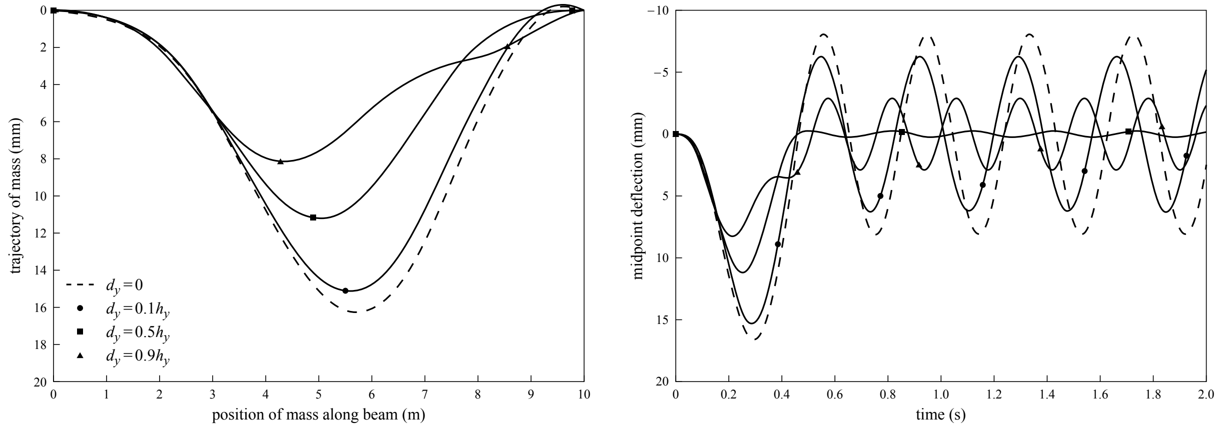

Figure 5. This figure presents similar information to that shown in Figure 4, except that the thickness ratios used are different with those shown in Figure 4.

the basic layer has lowest Young's modulus and largest density, increasing the thickness ratios $\hat{d}_y$ and $\hat{d}_z$ amplifies the capability of the beam to reduce the vibration of the system. However, if this is not the case, e.g., as those shown in Figure 6, large $\hat{d}_z$ may not have higher potential to diminish the amplitude of vibration than small $\hat{d}_z$. From Figures 6 and 7, one may conclude that the capability of the beam to diminish the vibration of the system increases with the stiffness ratio, but decreases with the density ratio, between the embedded and the basic layers.

Figure 8 presents the effects produced by the change of the number of strips and layers of the beam for set 1 (shown in dashed lines) and set 2 (shown in solid lines). In this figure, the beam deflection at mid-span when the mass reaches $\xi = 0.5$ is plotted as a function of the total of strips (Figure 8, left) and layers (Figure 8, right). In Figure 8 (left), two different beams are considered, a sandwich (symbolized by $+$) and a five-layer (symbolized by Δ) beams. The sandwich beam consists of one

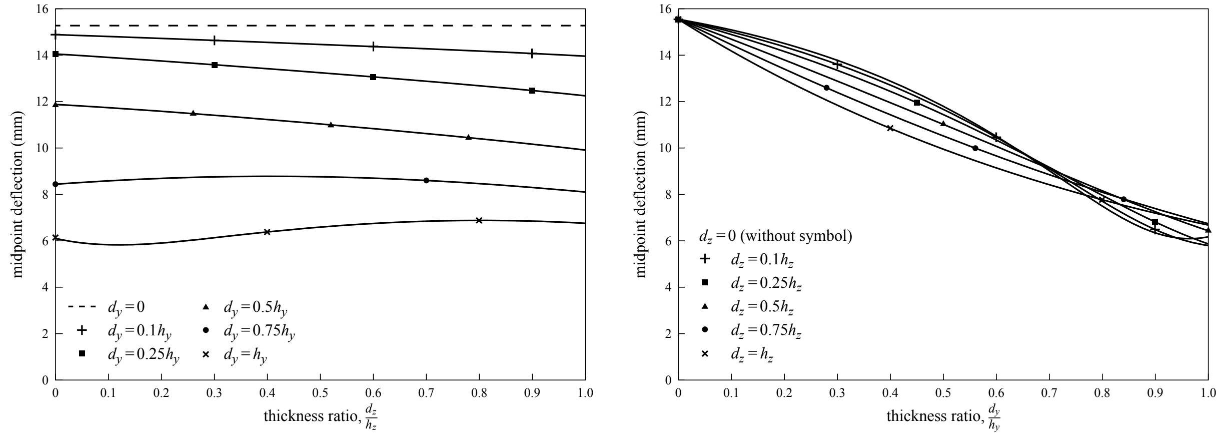

Figure 6. The midpoint deflection of the beam (mm) when the mass reaches the midpoint ($\xi = 0.5$) versus the variation of the thickness ratios $\hat{d}_z$ (left) and $\hat{d}_y$ (right).

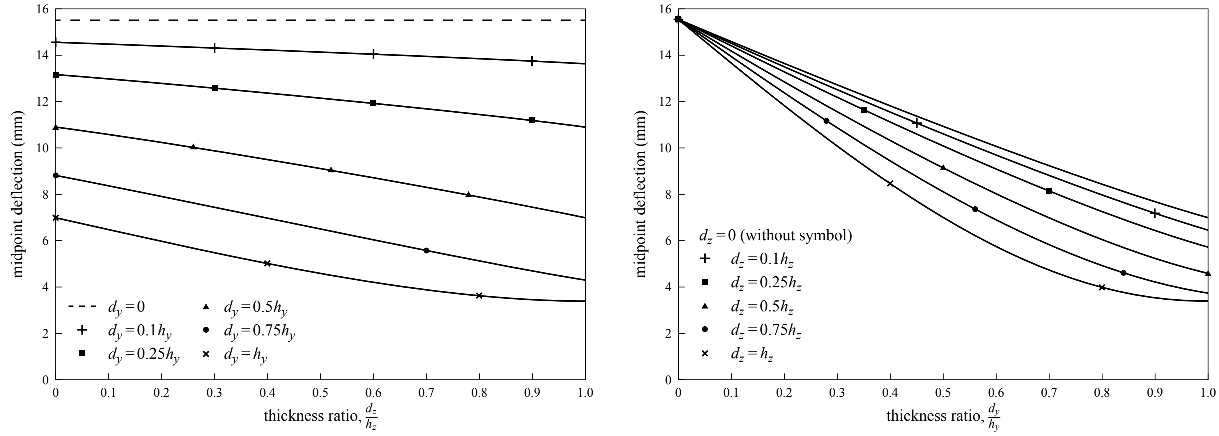

Figure 7. This figure presents similar information to that shown in Figure 6, except the set 2 being selected.

embedded and two basic layers; the five-layer beam is composed of three embedded and two basic layers. Both of the thickness ratios $\hat{d}_y$ and $\hat{d}_z$ are set to be 0.5. In Figure 8 (right), the number of strips of an embedded lamina chosen are 3 (symbolized by $+$) and 9 (symbolized by Δ). The two plots indicate that the difference due to different numbers of strips and layers converges quickly. Recalling that the increase of the number of strips and layers decreases the distance of the periods h_z and h_y, respectively. Therefore, for example, when the beam has a many of layers, the length of h_y becomes a tiny value and the terms $\hat{h}_y$ and $\hat{I}_y$ approach to zero such that $\hat{m}_{pq} \to \sum_{p=1}^{\infty} \hat{m}_p$ and $\hat{E}^t_{1jk} \to \sum_{j=1}^{\infty} \hat{E}_{1j}$ ((3) and (4b)). Similar phenomenon is also observed when $h_z(\hat{h}_z)$ is examined. This means that the midpoint deflection converges to a specific value as the number of strips and layers increases. From Figures 6–8, one concludes that with proper choice of the stiffness ratio, density ratio, and thickness ratio between the embedded and basic laminas of the beam, the growth of small amplitude vibration into large motion

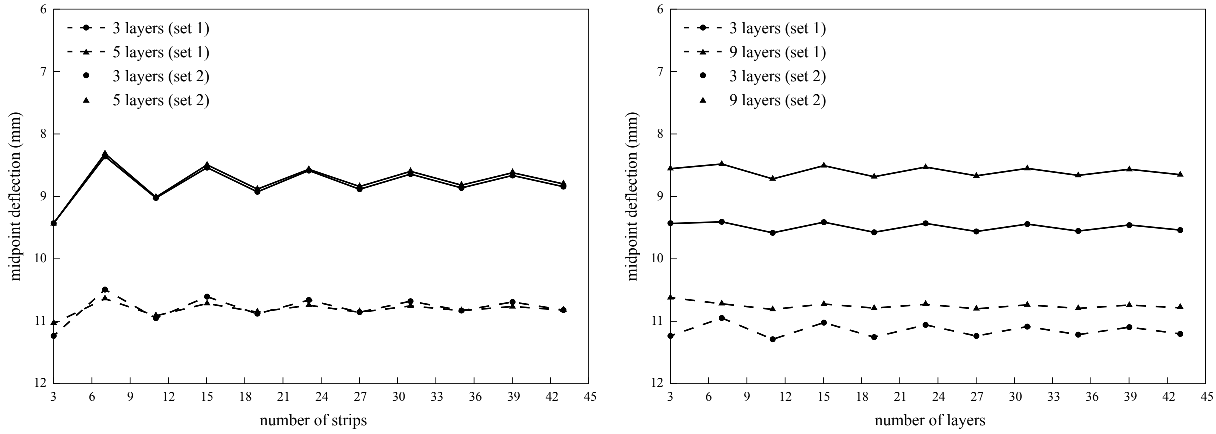

Figure 8. This figure shows the beam deflection at mid-span when the mass reaches $\xi = 0.5$ versus the number of strips of the embedded lamina (left) and the total of layers of the beam (right).

regime can be attenuated. In other words, because of inhomogeneity of materials, when structures are subjected to external excitations, structures have the ability to prolong their useful life by adjusting the arrangement of material and geometric properties between the embedded periodic-array and basic layers.

In the following, the mass slows down during operation being taken into account. Figure 9 illustrates the trajectory of mass (mm) versus the position of mass along a sandwich beam for different arrangements of periodic arrays and sets of parameters. The embedded lamina consists of three and two strips of a and b, respectively. The dashed and solid lines denote the set 1 and set 2, respectively. The thickness ratios $\hat{d}_y$ and $\hat{d}_z$ selected are: $\hat{d}_y = \hat{d}_z = 0$ (dashed line, without symbol), $\hat{d}_y = \hat{d}_z = 0.5$ (symbolized by $+$), $\hat{d}_y = 1$ and $\hat{d}_z = 0.5$ (symbolized by $\square$). In Figure 9 (left), the mass travels at constant speed, $v = 20\,\mathrm{m/s}$. In Figure 9 (right), the mass is under deceleration for $v_0 = 20\,\mathrm{m/s}$ (initial speed), $\mu = 0$ (zero friction), and $f = -20\,\mathrm{m/s}^2$ (the retard force applied on the mass). Figure 10 presents similar information to that shown in Figure 9 (right), except that the mass stops before the end support being considered. The initial speed and retard force applied on the mass are, respectively, $v_0 = 20\,\mathrm{m/s}$ and $f = -22\,\mathrm{m/s}^2$. The frictions used in Figure 10 (left) and Figure 10 (right) are $\mu = 0$ and $\mu = 0.5$, respectively. Note that the friction is served as another braking system and therefore it may not be a small value. These two figures clearly disclose that the periodic-array composite beam noticeably diminishes the amplitude of the trajectory of mass. Meanwhile, Figure 10 shows that as the mass is slowing down and stops prior to the terminal point, acute oscillation of the trace of mass occurs. In addition, when the mass is subjected to large reverse forces and friction force, the mass may stop away from the end support; under such situation, as the mass moves along a homogeneous beam (showing as dashed line without symbol) and is near the halt point, the oscillating amplitude of the trajectory of mass may become large. This condition can be avoided if the proposed beam is employed.

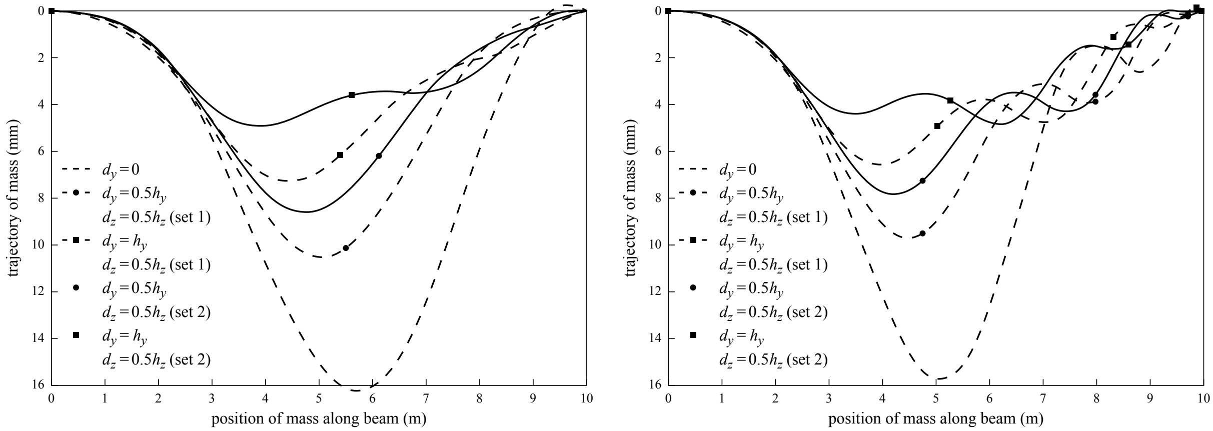

Figure 9. This figure illustrates the trajectory of mass (mm) versus the position of mass along the sandwich beam for different arrangements of periodic arrays. Left: the mass travels at constant speed. Right: the mass is under deceleration.

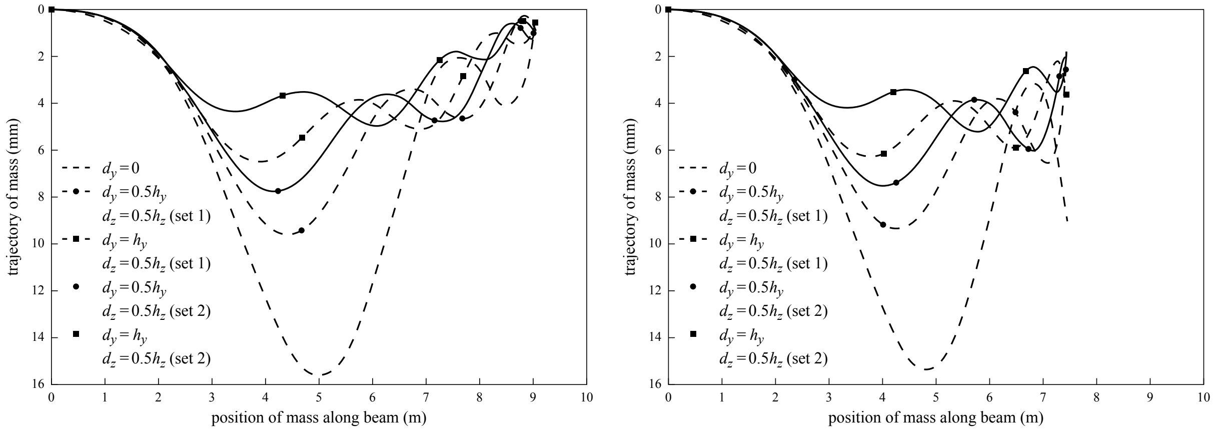

Figure 10. This figure presents similar information to that shown in Figure 9 except that the mass stops before the end terminal being considered with frictions $\mu = 0$ (left) and $\mu = 0.5$ (right).

4. Conclusions

In this study, nonhomogeneous beams having transversely periodic arrays and different arrangements of materials and laminas are considered. The Fourier series with a wavelength equal to the average space between two different strips and a wavelength equivalent to the average space between embedded and basic layers are used to take into account the periodicity of the embedded lamina and beam, respectively. The Young's modulus and density of the composite beam are biaxial periodic functions. The proposed passive nonhomogeneous beam is introduced to a beam-mass system to attenuate the likelihood of large-amplitude vibrations.

Results show that even if the material damping is not considered, the proposed beam has excellent capability to reduce the vibration of a beam-mass system after the mass left the beam. Different arrangements of material and geometric properties of the periodic arrays result in different bending stiffness and mass distribution of the beam. The vibration of the system can be effectively attenuated by properly choosing the stiffness and density ratios between the embedded strips/laminas and basic layers. It indicates that the bending frequency of the nonhomogeneous beam varies with the change of mass ratio, Young's modulus ratio, and thickness ratio of the periodic arrays; this is not observed when a homogeneous beam is taken into account. In addition, the proposed model may be applied to many applications if proper materials are selected. For example, if the shape-memory-alloy (SMA) is used to replace the strip a, the beam is capable of having the ability to overcome the influence produced by the change of temperature.

Acknowledgements

The authors wish to express their sincere appreciation to the reviewers for their valuable comments.

Table of notations

H: height of the beam (gravitational (y) direction)

W: width of the beam (horizontal (z) direction)

I: the area moment of inertia of the beam

$\widetilde{M}$: the resultant bending moment about the neutral axis of the cross-section of the beam at time t

M, $\widehat{M}$: the mass and the dimensionless mass of the moving mass

N, $\widehat{N}$: the dimensional and nondimensional normal reaction force between the beam and the riding mass

T: the axial force in the beam

V: the transverse force in the beam

a, b, c: material symbols of the two different strips used in an embedded lamina and the basic layers, respectively

f: the thrust applied on the riding mass

m: mass per unit length of the beam

ℓ: length of the beam

E_a, E_b, E_c: the Young's moduli of the strips a, b, and the basic layer, respectively

E_1^z: the axial Young's modulus of an embedded lamina, a periodic function in z direction

$E_1(y, z)$: the axial Young's modulus of the nonhomogeneous beam, a biaxial periodic function in y and z directions

d_y, $\hat{d}_y$: one-half of the thickness of an embedded lamina and the thickness ratio of an embedded lamina being present in one period ($2h_y$) in the height direction, $\hat{d}_y = d_y/h_y$, respectively

d_z, $\hat{d}_z$: one-half of the thickness of the strip a and the thickness ratio of the strip a being present in one period ($2h_z$) in the width direction, $\hat{d}_z = d_z/h_z$, respectively

h_y, $\hat{h}_y$: one-half of the distance between the midpoint of two basic layers separated by one embedded lamina and the ratio of $2h_y$ to the height of the beam, $\hat{h}_y = 2h_y/H$, respectively

h_z, $\hat{h}_z$: one-half of the distance between the midpoint of two strips of b separated by one ply of a and the ratio of $2h_z$ to the width of the beam ($\hat{h}_z = 2h_z/W$), respectively

s, $\bar{s}$: the arc length and the position of the moving mass along the beam, respectively

u: the axial displacement of the beam measured from the undeformed state

v: the transverse displacement of the beam measured from the undeformed state

ρ_a, ρ_b, ρ_c: densities of the strips a, b, and the basic layer, respectively

ρ^z: density of an embedded lamina, which is a periodic function in z direction, $\rho^z = \rho^z(z)$

ρ: density of the nonhomogeneous beam, which is a biaxial periodic function in y and z directions, $\rho = \rho(y, z)$

$\boldsymbol{a}_M$: acceleration of the moving mass

$\boldsymbol{f}$: the external forces including the weight and the reactions of the moving mass upon the composite beam

$\boldsymbol{g}$: acceleration due to gravity ($= g\boldsymbol{j}$)

$\boldsymbol{I}$: the $n \times n$ unit matrix

$\boldsymbol{i}$: the unit vector in the horizontal direction

$\boldsymbol{j}$: the unit vector in the gravitational (transverse) direction

$\boldsymbol{n}$: the unit normal vector to the beam configuration

$\boldsymbol{r}$: the Cartesian position vector of point s along the beam at time t

$\hat{\boldsymbol{\tau}}$: the unit tangent vector to the beam configuration

μ: coefficient of friction

ξ: dimensionless position of the moving mass along the beam

ω_j^h: the normalized frequency of the j-th mode vibration of the homogeneous beam

$\bar{\delta}(s - \bar{s})$: Dirac delta function

δ_{rp}: Dirac delta symbol

References

[Şimşek 2010] M. Şimşek, "Vibration analysis of a functionally graded beam under a moving mass by using different beam theories", *Compos. Struct.* **92** (2010), 904–917.

[Şimşek and Kocatürk 2009] M. Şimşek and T. Kocatürk, "Free and forced vibration of a functionally graded beam subjected to a concentrated moving harmonic load", *Compos. Struct.* **90**:4 (2009), 465–473.

[Şimşek et al. 2012] M. Şimşek, T. Kocatürk, and Ş. D. Akbaş, "Dynamic behavior of an axially functionally graded beam under action of a moving harmonic load", *Compos. Struct.* **94**:8 (2012), 2358–2364.

[Friswell and Lees 2001] M. I. Friswell and A. W. Lees, "The modes of non-homogeneous damped beams", *J. Sound Vib.* **242**:2 (2001), 355–361.

[Han et al. 1999] S. M. Han, H. Benaroya, and T. Wei, "Dynamics of transversely vibrating beams using four engineering theories", *J. Sound Vib.* **225**:5 (1999), 935–988.

[Kahya and Turan 2018] V. Kahya and M. Turan, “Vibration and stability analysis of functionally graded sandwich beams by a multi-layer finite element”, *Compos. B Eng.* **146** (2018), 198–212.

[Lee and Lee 2017] J. W. Lee and J. Y. Lee, “Free vibration analysis of functionally graded Bernoulli-Euler beams using an exact transfer matrix expression”, *Int. J. Mech. Sci.* **122** (2017), 1–17.

[Li et al. 2008] J. Li, H. Hua, and R. Shen, “Dynamic stiffness analysis for free vibrations of axially loaded laminated composite beams”, *Compos. Struct.* **84**:1 (2008), 87–98.

[Misiurek and Śniady 2013] K. Misiurek and P. Śniady, “Vibrations of sandwich beam due to a moving force”, *Compos. Struct.* **104** (2013), 85–93.

[Mohebpour et al. 2016] S. R. Mohebpour, M. Vaghefi, and M. Ezzati, “Numerical analysis of an inclined cross-ply laminated composite beam subjected to moving mass with consideration the Coriolis and centrifugal forces”, *Eur. J. Mech. A Solids* **59** (2016), 67–75.

[Rao et al. 2001] M. K. Rao, Y. M. Desai, and M. R. Chitnis, “Free vibrations of laminated beams using mixed theory”, *Compos. Struct.* **52**:2 (2001), 149–160.

[Sayyad and Ghugal 2017] A. S. Sayyad and Y. M. Ghugal, “Bending, buckling and free vibration of laminated composite and sandwich beams: a critical review of literature”, *Compos. Struct.* **171** (2017), 486–504.

[Sheng and Wang 2018] G. G. Sheng and X. Wang, “Nonlinear vibration of FG beams subjected to parametric and external excitations”, *Eur. J. Mech. A Solids* **71** (2018), 224–234.

[Song et al. 2018] Q. Song, Z. Liu, J. Shi, and Y. Wan, “Parametric study of dynamic response of sandwich plate under moving loads”, *Thin-Walled Struct.* **123** (2018), 82–99.

[Tao et al. 2016] C. Tao, Y.-M. Fu, and H.-L. Dai, “Nonlinear dynamic analysis of fiber metal laminated beams subjected to moving loads in thermal environment”, *Compos. Struct.* **140** (2016), 410–416.

[Wang 2009] Y.-M. Wang, “The transient dynamics of a moving accelerating/decelerating mass traveling on a periodic-array non-homogeneous composite beam”, *Eur. J. Mech. A Solids* **28** (2009), 827–840.

Received 23 Jun 2018. Revised 28 Jan 2019. Accepted 18 Apr 2019.

YI-MING WANG: `wangym@cc.ncue.edu.tw`
Department of Mechatronics Engineering, National Changhua University of Education, 2 Shih-Ta Road, Changhua 500, Taiwan

HUNG-CHIEH LIU: `d0351005@mail.ncue.edu.tw`
Department of Mechatronics Engineering, National Changhua University of Education, 2 Shih-Ta Road, Changhua 500, Taiwan

JOURNAL OF MECHANICS OF MATERIALS AND STRUCTURES

msp.org/jomms

Founded by Charles R. Steele and Marie-Louise Steele

EDITORIAL BOARD

Adair R. Aguiar	University of São Paulo at São Carlos, Brazil
Katia Bertoldi	Harvard University, USA
Davide Bigoni	University of Trento, Italy
Maenghyo Cho	Seoul National University, Korea
Huiling Duan	Beijing University
Yibin Fu	Keele University, UK
Iwona Jasiuk	University of Illinois at Urbana-Champaign, USA
Dennis Kochmann	ETH Zurich
Mitsutoshi Kuroda	Yamagata University, Japan
Chee W. Lim	City University of Hong Kong
Zishun Liu	Xi'an Jiaotong University, China
Thomas J. Pence	Michigan State University, USA
Gianni Royer-Carfagni	Università degli studi di Parma, Italy
David Steigmann	University of California at Berkeley, USA
Paul Steinmann	Friedrich-Alexander-Universität Erlangen-Nürnberg, Germany
Kenjiro Terada	Tohoku University, Japan

ADVISORY BOARD

J. P. Carter	University of Sydney, Australia
D. H. Hodges	Georgia Institute of Technology, USA
J. Hutchinson	Harvard University, USA
D. Pamplona	Universidade Católica do Rio de Janeiro, Brazil
M. B. Rubin	Technion, Haifa, Israel

PRODUCTION production@msp.org

Silvio Levy Scientific Editor

Cover photo: Mando Gomez, www.mandolux.com

See msp.org/jomms for submission guidelines.

JoMMS (ISSN 1559-3959) at Mathematical Sciences Publishers, 798 Evans Hall #6840, c/o University of California, Berkeley, CA 94720-3840, is published in 10 issues a year. The subscription price for 2019 is US $635/year for the electronic version, and $795/year (+$60, if shipping outside the US) for print and electronic. Subscriptions, requests for back issues, and changes of address should be sent to MSP.

JoMMS peer-review and production is managed by EditFlow® from Mathematical Sciences Publishers.

PUBLISHED BY
mathematical sciences publishers
nonprofit scientific publishing
http://msp.org/

© 2019 Mathematical Sciences Publishers

Journal of Mechanics of Materials and Structures

Volume 14, No. 2 March 2019

A mode-dependent energy-based damage model for peridynamics and its implementation
CHRISTIAN WILLBERG, LASSE WIEDEMANN and MARTIN RÄDEL 193

Elastic wave propagation in a periodic composite plate structure: band gaps incorporating microstructure, surface energy and foundation effects
GONGYE ZHANG and XIN-LIN GAO 219

Dynamic analysis of a mass traveling on a simply supported nonhomogeneous beam composed of transversely embedded periodic arrays
YI-MING WANG and HUNG-CHIEH LIU 237

Stress concentration around an arbitrarily-shaped hole in nonlinear fully coupled thermoelectric materials
CHUAN-BIN YU, HAI-BING YANG, KUN SONG and CUN-FA GAO 259

The effect of variable thermal conductivity on an infinite fiber-reinforced thick plate under initial stress
MOHAMED I. A. OTHMAN, AHMED E. ABOUELREGAL and SAMIA M. SAID 277

Large deflections and stability of spring-hinged cantilever beam MILAN BATISTA 295

1559-3959(2019)14:2;1-W